Comparison of flux observers for sensorless control of permanent magnet assisted SynRel motors

Comparison of Flux Observers for Sensorless Control of Permanent Magnet Assisted SynRel Motors

Luca Concari, Andrea Toscani, Davide Barater, Carlo Concari
DII, University of Parma, Parma, Italy
luca.concari2@studenti.unipr.it, andrea.toscani@unipr.it, davide.barater@unipr.it, carlo.concari@unipr.it

Michele Degano
The University of Nottingham, Nottingham, UK
michele.degano@nottingham.ac.uk

Gianmario Pellegrino
Dipartimento Energia
Politecnico di Torino, Turin, Italy
gianmario.pellegrino@polito.it

***Abstract*— This paper proposes the comparison among different sensorless position estimation strategies suitable for permanent magnet assisted synchronous reluctance machine drives. A machine of such type was designed and optimized aiming at improving its sensorless performance, besides minimizing the torque ripple and maximizing the power factor. Different sensorless solutions for the estimation of the magnetic flux linkage and for tracking the rotor angle are investigated and their performance compared in computer simulations. Experimental results are reported for the PM-assisted synchronous reluctance motor drive example.**

Keywords—Permanent magnet assisted synchronous reluctance machines, PMaSynRel drives, sensorless control techniques, magnetic flux observers.

I. INTRODUCTION

The continuous increase of electrical energy demand compels a significant effort in the direction of reducing the related environment pollution and greenhouse effect. Therefore, it has become mandatory to improve the efficiency of electric motors used in many application fields [1]. New standards on rotating electrical machines are way more demanding than in the past, in terms of efficiency. Presently, the Synchronous Reluctance (SynRel) motor appears to be one of the most attractive emerging electrical machine technologies. Suitable for vehicle traction [1]-[4], [9], industrial applications and household appliances [5], these motors present excellent features such as a robust structure, very high-speed capabilities, absence of excitation winding and low back electro motive force, leading to a safe behavior in case of inverter failure. On the contrary, the well-known drawback of reluctance machines is the poor power factor and the attitude to producing non-negligible torque ripple [6]. To compensate for these downsides and to maximize the motor performance, an optimized design of the entire drive is always required [6], [8]. Furthermore, the power factor and the machine torque density can be improved with addition of limited quantities of rare-earth magnet or low-cost ferrite magnet, resulting in the so-called Permanent Magnet assisted Synchronous Reluctance (PMaSynRel) configurations [8]. Respect to induction machines with the same frame size, the PMaSynRel machines exhibit a higher torque density and efficiency, over a wide operating speed range [5].

Because of their anisotropic rotor structure, PMaSynRel motors are also suitable for zero-speed sensorless control, with all the benefits related to the absence of any kind of mechanical transducer [10]. Also, they easily allow flux weakening if PM flux amount is negligible compared to the rated flux, since in this case the flux is mainly controlled by the stator currents.

This paper is divided in two parts. The first part describes the design of the electric motor, its main features and the determination of the preliminary magnetic model used to implement the control strategy on the experimental platform drive. The second part is dedicated to the comparison of three sensorless position estimation strategies. Experimental results are presented for the sake of validation of the simulation results. The analysis identifies the best control strategy, and the data required from the motor design stage to have appropriate control performance, in sensorless operation.

II. MOTOR DESIGN AND MAGNETIC MODEL

The design of the machine is briefly introduced in this section, highlighting the main features that have been optimized with the aim of simplifying the sensorless control for both low and high speed operation mode. The magnetic model determined through Finite Element (FE) Analysis and used for the initial tuning of the control parameters is described in subsection B.

A. Electrical machine design

A PM assisted SynRel machine was designed for a power and speed rating that suits well a motor to be used for household appliances. The stator is that of a commercial induction motor, with 24 slot and distributed windings. The 4 pole rotor of the induction machine was replaced with a new design made of an anisotropic structure like the one shown in Fig.1, maintaining the same number of poles and thus the same winding configuration. The rotor has three flux barriers per pole, with the central parts of the barriers filled with ferrite permanent magnet, having the function of assisting the saturation of the radial and tangential iron ribs. Their

dimensions were determined through a mechanical model in order to obtain a robust rotor and preserve the structure subject to centrifugal forces when the machine is running at high speed. Thanks to the high anisotropy of the rotor, this machine is well suited for sensorless operation and position detection even down to zero speed. Given the 24-slot stator lamination geometry, the rotor was designed considering a peak current density in the slot fixed to J_{MAX} = 4.5 A_{RMS}/mm^2 and a fill factor assumed to be k_{fill} = 0.4. The geometry was designed and optimized by means of 2*D* FE models. The final machine is reported in Fig. 1. The design strategy aimed to achieve the rated torque T_n, taking full advantage of the iron $B-H$ characteristics of the silicon steel commercial laminations M470-50A. After optimization of the rotor laminations geometry, a torque ripple of 7.3% is achieved at rated torque. Motor parameters are given in TABLE I.

B. *PMaSynRel magnetic model*

The *dq* reference frame was chosen following the SynRel conventions. The *d-axis* is aligned with the maximum permeance direction, as represented in Fig. 1. Consequently, the PM flux linkage is aligned to the negative *q-axis* direction. The magnetic model was obtained with finite element simulations. The motor parameters were determined post processing the results of the FE analysis. Fig. 2 reports the magnetic flux−current and inductance−current characteristics, obtained with the FE simulations. As can be noted, the cross saturation effect influences the motor parameters significantly: separation of the flux curves is due to the current component on the other axis. The simplest way of taking into account the cross saturation, is to store the magnetic model of the machine into two bi-dimensional look-up tables representing $\lambda_d = f(i_d, i_q)$ and $\lambda_q = f(i_d, i_q)$. The current space vector trajectory was evaluated according to the Maximum Torque Per Ampere (MTPA) locus and Flux Weakening (FW) up to the maximum speed (12000 *rpm*). Varying the *d*– and *q*– axis currents and computing the *d*– and *q*– axis flux linkages and torque, allowed to identify the most convenient trajectory on the $i_d - i_q$ space, depicted in Fig. 3. It is worth noticing that the FW trajectory for this PMaSynRel motor drive does not include the Maximum Torque Per Volt (MTPV) locus. The resultant base speed is around 4500 *rpm*.

TABLE I. MOTOR PARAMETERS

Power	700 W
Phase Voltage (rms)	120 V
Phase Current (rms)	3.5 A
Base speed	4500 rpm
Maximum speed	12000 rpm
Rated torque	1.5 Nm
Pole Pairs	2

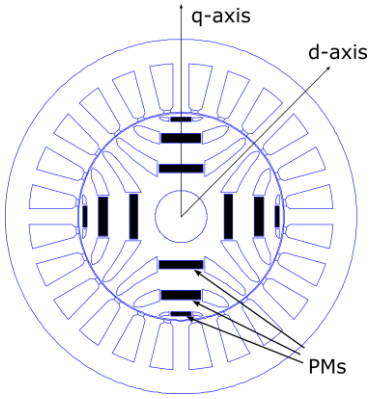

Fig. 1. 2D sketch of a ferrite assisted synchronous reluctance machine.

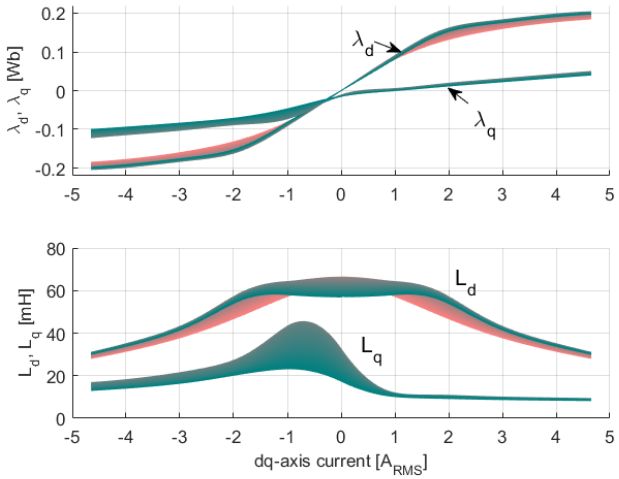

Fig. 2. *Magnetic flux−current and inductance−current characteristics computed through FE simulations.*

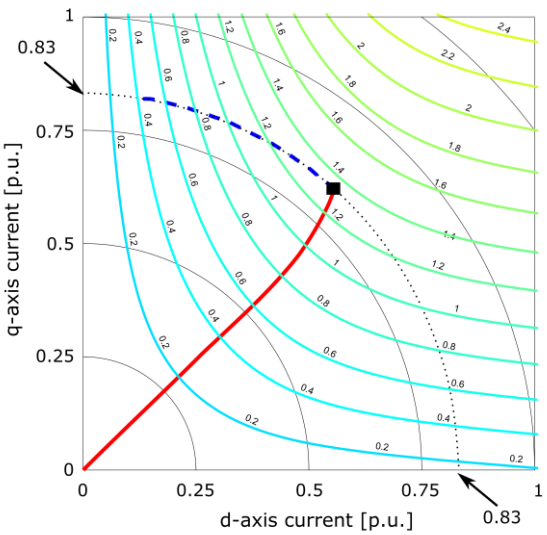

Fig. 3. *MTPA (red) and FW (blue) trajectory computed through FE simulations.*

III. PMaSynRel Control Scheme

The control strategy is based on an ordinary current vector control in the dq axes, depicted in Fig. 4. The outer loop performs a speed control, and the speed measurement may come from either a physical sensor or a sensorless algorithm. The output of the speed regulator is the modulus of the current.

The i_d^* and i_q^* current set-points, which feed the inner current control loops, are computed from their modulus using two look-up tables derived from the MTPA (maximum torque per ampere) trajectory, when possible, or a voltage limited trajectory when in the flux weakening speed range.

FE simulations of the designed motor have been used to determine the optimum trajectory on the $i_d - i_q$ frame for different rotor speeds, from zero to the maximum (12000 rpm). As shown in Fig. 3, the MTPA curve in i_d and i_q components resembles a straight line at an angle of 45°. Therefore the control strategy at low speed will impose that i_d and i_q are equal to each other, to meet the MTPA condition. Increasing speed over the base value requires that the circular trajectory (blue curve in Fig. 3) is respected, with constant current modulus, up to the maximum speed The functions manipulating the current references at the different speeds are represented in Fig. 5:the i_d^*, i_q^* current set-points follow the strategy of Fig. 5. As said, the first section was approximated with a straight segment oriented at 45°, then $f_1(\omega) = i_d \,/\, |i|$ and $f_2(\omega) = i_q \,/\, |i|$ were derived by model manipulation in continuity with the MTPA trajectory of Fig. 3.

In order to prevent output voltage distortion due to saturation of the duty-cycle, prior to Park and Clarke inverse transformations, the dq voltage is saturated so that the angle of the vector is preserved, even when the amplitude is saturated.

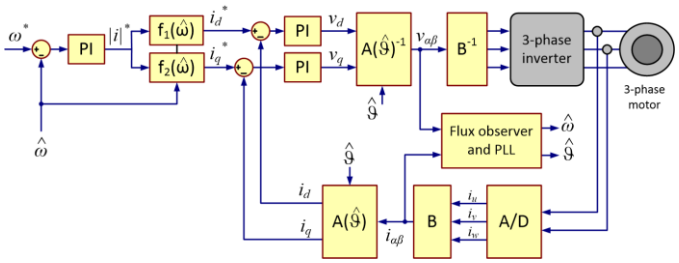

Fig. 4. *PMaSynRel control scheme.*

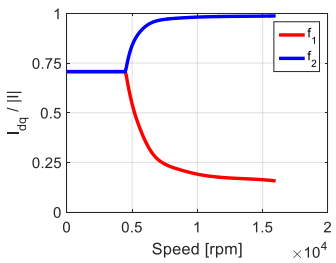

Fig. 5. *Ratios between dq current components and current modulus versus rotor speed along MTPA trajectory.*

The adopted vector control scheme needs the knowledge of the rotor angular position and speed. In sensored solutions these come from a physical sensor, typically an encoder or a resolver, while in sensorless schemes they must be obtained with some type of software observer able to track the rotor position [11]. Three sensorless methods were investigated, as reported in Section IV.

IV. PMaSynRel Sensorless Control

As stated above, in order to implement a sensorless control strategy it is necessary to track the angle of the rotor. Three different solutions for the position estimation algorithm were investigated and are reported below.

A. Permanent Magnets Flux Observer

This observer estimates the rotor position tracking the phase angle of the flux linkage produced by permanent magnets, that is in phase with the negative q-axis of the rotor. The idea is that this flux is given by the difference (1), where $\hat{\lambda}_{\alpha\beta}$ is the total estimated flux, computed by integrating the back-emf on $\alpha\beta$ axes, and $\tilde{\lambda}^L_{\alpha\beta}$ is obtained using the magnetic model (on dq axes) of the motor without permanent magnets contribution, that is without the offset in the $\tilde{\lambda}_q(i_d, i_q)$ characteristics. Superscript L denotes the inductance related component of the magnetic flux.

$$\hat{\lambda}^M_{\alpha\beta} = \hat{\lambda}_{\alpha\beta} - \tilde{\lambda}^L_{\alpha\beta} \tag{1}$$

The angle ϑ used in Park $A(\vartheta)$ and inverse Park $A^T(\vartheta)$ transformation is self-supplied by the observer.

The major problem with this method is that $\lambda_{\alpha\beta}$ and $\lambda'_{\alpha\beta}$ are quite similar, so $\lambda^M_{\alpha\beta}$ results to be small and affected by the estimation error of $\lambda'_{\alpha\beta}$.

B. Sliding Mode Observer (SMO)

This sensorless strategy is based on a modified version of the Sliding Mode Observer (SMO) to estimate the rotor position and perform sensorless operation [12].

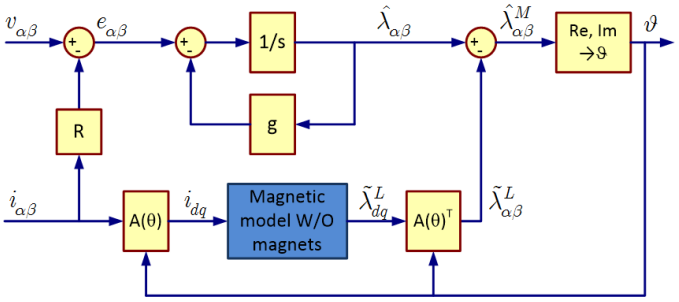

Fig. 6. *Permanent Magnets Flux Observer block scheme.*

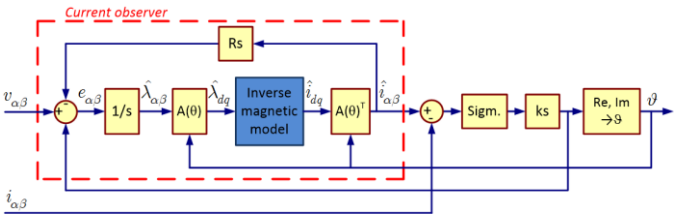

Fig. 7. *Sliding mode observer scheme.*

The most important part of this scheme is the current observer, based on the inverse magnetic model $i_{dq} = f\ \lambda_{dq}$. The motor flux $\hat{\lambda}_{\alpha\beta}$ on the $\alpha\beta$ axes, estimated through the integration of the back-emfs, is used to compute $\hat{\lambda}_{dq}$. This flux indexes a two-dimensional look-up table that gives the currents $\hat{i}_{dq}$, then, with a reverse Park $A^T(\vartheta)$ matrix, returns $\hat{i}_{\alpha\beta}$.

The conventional SMO uses the sign function as switching function, and a low-pass filter (LPF) eliminates the chattering effect. In the proposed solution, this task is done with a different function to reduce the computational load of the algorithm.

$$H(x) = \left\{ \frac{1}{1 + e^{-kx}} - 1 \right\} \tag{2}$$

Also in this scheme the angle ϑ used in the Park $A(\vartheta)$ and inverse Park $A^T(\vartheta)$ transformations is self-supplied by the observer.

C. Hybrid flux observer

The upper part of this observer estimates the flux $\lambda_{\alpha\beta}$ integrating the back-emfs, while the lower part relies on the magnetic model of the motor. The two contributions are added with a frequency-dependent weight [13].

$$\hat{\lambda}_{\alpha\beta} = \frac{s}{s+g} \cdot \left(\frac{v_{\alpha\beta} - R \cdot i_{\alpha\beta}}{s} \right) + \frac{g}{s+g} \cdot \tilde{\lambda}_{\alpha\beta} \tag{3}$$

At higher frequencies the most important contribution is that given by back-emf integration (the term $s\ /\ (s+g)$ is a high pass filter, HPF), while at lower frequencies the most important contribution is given by the magnetic model (the term $g\ /\ (s+g)$ is a low pass filter, LPF).

The sum of the coefficients that represent the weights of the two contributions is always one.

The magnetic model of the motor is implemented as a bi-dimensional look-up table $\tilde{\lambda}_{dq} = f\ \ i_{dq}$.

Since the flux vector λ_{dq}, and its observed counterpart $\hat{\lambda}_{dq}$, on the rotating dq frame have, in general, an angle different from zero, tracking the flux vector produces an error in the estimation of the rotor angle ϑ, which is the displacement between the $\alpha\beta$ and dq reference frames needed by the Park's transformations (Fig. 8). A correction was introduced in order to overcome this problem, evaluating ϑ as stated in (4), where ϑ'' represents the flux angle in the rotating frame dq and ϑ' is the angle of the same flux in the stationary frame $\alpha\beta$.

$$\vartheta = \vartheta' - \vartheta'' \tag{4}$$

In the following, the strategy adopting this correction is addressed as "hybrid flux observer with compensation".

The whole observer (integrated back-emf and model-based branches) estimates the magnetic flux on the $\alpha\beta$ axes, but the proposed improvement needs the flux in the dq frame. So it becomes necessary to add a Park's transformation as shown in Fig. 9.

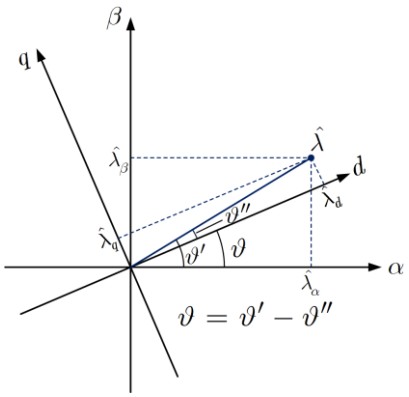

Fig. 8. *Relationship between the angle of the flux vector and that of the dq reference frame.*

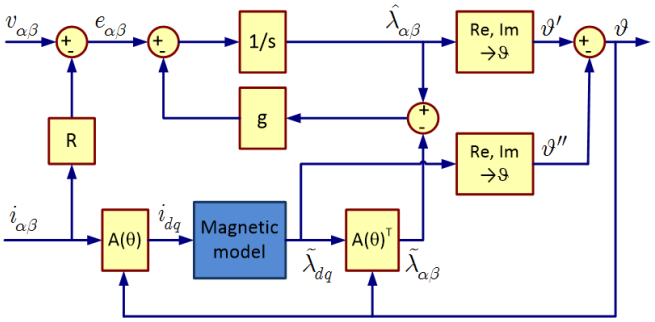

Fig. 9. *Scheme of the hybrid flux observer with compensation.*

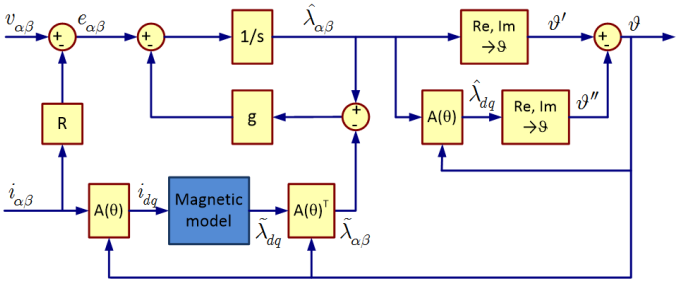

Fig. 10. *Scheme of the simplified hybrid flux observer with compensation.*

A simplified version of the observer relies on the usage of $\hat{\lambda}_{dq}$ (available at the magnetic model output) and allows to avoid the transformation block, thus reducing the calculation time in the final implementation. Furthermore, considering the magnetic behavior of the motor, in all the practical working conditions $\lambda_d \gg \lambda_q$, so that (5) can be approximated with (6). This allows to implement the $\mathrm{Re}, \mathrm{Im} \rightarrow \vartheta''$ block with only one division.

$$\vartheta'' = \arg(\tilde{\lambda}_{dq}) = \arctan\left(\frac{\tilde{\lambda}_q}{\tilde{\lambda}_d}\right) \tag{5}$$

$$\vartheta'' \simeq \frac{\tilde{\lambda}_q}{\left|\tilde{\lambda}_{dq}\right|} \simeq \frac{\tilde{\lambda}_q}{\tilde{\lambda}_d} \tag{6}$$

In all the three previous observers the $\mathrm{Re}, \mathrm{Im} \rightarrow \vartheta$ blocks were implemented with a phase-locked loop (PLL).

V. Simulation Results

A Matlab/Simulink model was adopted for the comparison of the investigated observers, featuring the magnetic model of the motor and performing the control strategy of Fig. 4. Simulations were conducted with a rotor speed of 2000 rpm at rated torque.

The flux observer block was implemented in the three different ways described in the previous section. All of them present good performance tracking of the rotor angle ϑ, as shown in Fig. 11. All the traces are substantially superimposed, however, a small angular displacement exists for each of them.

The error with respect to the actual rotor position (i.e. as sensed by a position transducer) is displayed in Fig. 12. The rms values of the errors over three electric periods are reported in TABLE II. As can be seen, the SMO exhibits the highest error (10.76°), while the lowest mean error of -0.41° comes from the hybrid flux observer with the compensation of the flux vector angle in the *dq* reference frame, which presents both the lowest rms error and almost no oscillation.

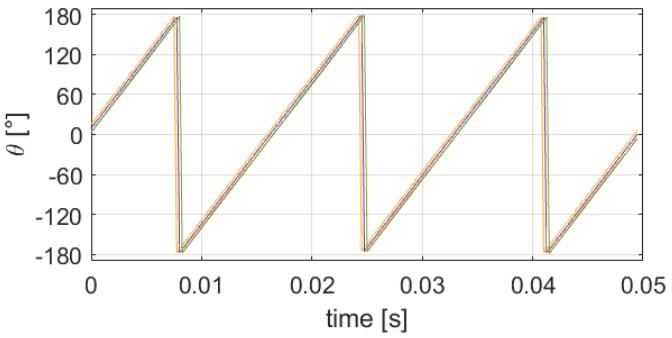

Fig. 11. *Tracked angle for the investigated observers, over three electric periods.*

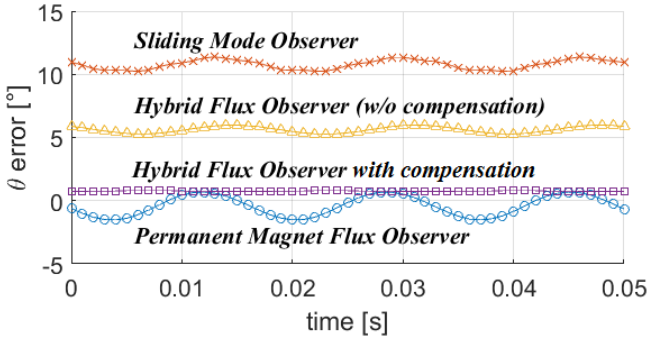

Fig. 12. *Tracking errors for the investigated flux observers.*

TABLE II. RMS VALUES OF THE TRACKING ERRORS

Observer type	Error (rms)
Permanent Magnets Flux Observer	0.85°
Sliding Mode Observer (SMO)	10.8°
Hybrid flux observer (without compensation)	5.6°
Hybrid flux observer with compensation	0.76°

VI. Experimental Results

In order to validate the effectiveness of the investigated observers, experiments were performed on the PMaSynRel machine mechanically coupled with a personal computer (PC)-controlled load machine. The motor was driven by a three-phase voltage PWM inverter featuring the smart power module STK5Q4U362J from On Semiconductor (10 A, 600 V), controlled by the 32-bit Toshiba TMPM375 microcontroller, with a 20 kHz PWM frequency. Rotor position was measured by means of an encoder.

The experimental board also contains a SPI interface, which is used for connection with an external digital-to-analog converter (DAC) for monitoring the control variables evolution. A simplified scheme of the setup is shown in Fig. 13. The adopted motor features a rated torque of 1.5 Nm up to 4500 rpm and a maximum speed of 12000 rpm reachable through flux weakening.

The focus of this work is on the sensorless techniques, i.e. the validation of the flux observer performance in tracking the rotor position and, consequently, the speed. Tests were carried out adopting for the flux observer the best performing one from the simulations, that here is presented as the “hybrid flux observer with compensation”. The correspondence between the tracked angle from the observer and that one reconstructed from the encoder signals was examined. Fig. 14 depicts the angle evolution at 4000 rpm that confirms the simulated results. The angle from the Hybrid flux observer without the proposed compensation (magenta trace) exhibits an error of about 5°, while the compensated one is almost free from errors (blue trace superimposed to the yellow trace from the encoder).

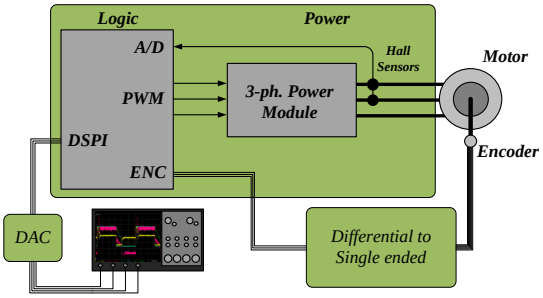

Fig. 13. *Scheme of the experimental drive.*

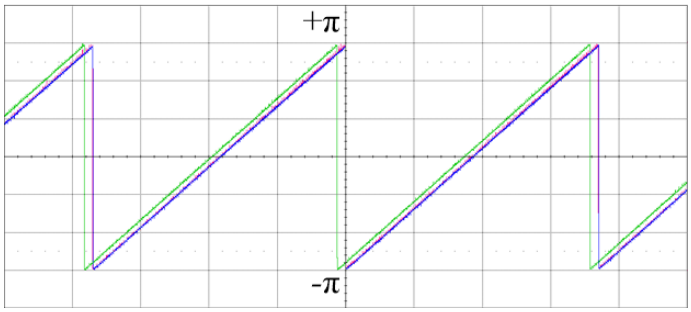

Fig. 14. *Tracked angle from the flux observer without (green) and with compensation (blue) superimposed to the encoder angle (magenta), time scale is 2ms/div. Rotor speed is 4000 rpm.*

VII. Conclusions

In this paper, three flux observer architectures for permanent magnet assisted synchronous reluctance machines were tested and compared by simulation. The one that performed better in simulation ("hybrid flux observer with compensation") was experimentally tested on a specially designed PMaSynRel machine, both with and without compensation of the flux vector angle in the *dq* reference frame. Experimental results confirm the results of the simulations and the good performance of the hybrid flux observer.

References

[1] A. T. de Almeida, F. J. T. E. Ferreira and G. Baoming, "Beyond Induction Motors—Technology Trends to Move Up Efficiency," in IEEE Transactions on Industry Applications, vol. 50, no. 3, pp. 2103-2114, May-June 2014.

[2] A. El-Refaie, J. Alexander, S. Galioto, P. Reddy, K.-K. Huh, P. de Bock, and X. Shen, "Advanced high-power-density interior permanent magnet motor for traction applications", IEEE Transactions on Industry Applications, vol. 50, no. 5, pp. 3235–3248, Sept 2014.

[3] E. Carraro, M. Degano, M. Morandin, and N. Bianchi, "Formula SAE electric competition: Electrical motor design", in IEEE International Electric Machines Drives Conference (IEMDC), May 2013, pp. 1142–1148.

[4] J. Tangudu and T. Jahns, "Comparison of interior PM machines with concentrated and distributed stator windings for traction applications", in IEEE Vehicle Power and Propulsion Conference (VPPC), 2011, pp. 1–8.

[5] A. De Almeida, F. Ferreira, and A. Quintino Duarte, "Technical and economical considerations on super high-efficiency three-phase motors", Industry Applications, IEEE Transactions on, vol. 50, no. 2, pp. 1274–1285, March 2014.

[6] N. Bianchi, M. Degano and E. Fornasiero, "Sensitivity Analysis of Torque Ripple Reduction of Synchronous Reluctance and Interior PM Motors," in IEEE Transactions on Industry Applications, vol. 51, no. 1, pp. 187-195, Jan.-Feb. 2015.

[7] S. Yamamoto, H. Hirahara, J. Adawey, T. Ara, and K. Matsuse, "Maximum efficiency drives of synchronous reluctance motors by a novel loss minimization controller with inductance estimator", Industry Applications, IEEE Transactions on, vol. 49, no. 6, pp. 2543–2551, Nov 2013.

[8] M. Degano, E. Carraro and N. Bianchi, "Selection Criteria and Robust Optimization of a Traction PM-Assisted Synchronous Reluctance Motor", in *IEEE Transactions on Industry Applications*, vol. 51, no. 6, pp. 4383-4391, Nov.-Dec. 2015.

[9] J. Malan and M. Kamper, "Performance of a hybrid electric vehicle using reluctance synchronous machine technology", IEEE Transactions on Industry Applications, vol. 37, no. 5, pp. 1319–1324, Sep 2001.

[10] I. Boldea et al., "DTFC-SVM motion-sensorless control of a PM-assisted reluctance synchronous machine as starter-alternator for hybrid electric vehicles", in IEEE Transactions on Power Electronics, vol. 21, no. 3, pp. 711-719, May 2006.

[11] G. Buticchi, E. Lorenzani, F. Immovilli and C. Bianchini, "Active Rectifier With Integrated System Control for Microwind Power Systems," in *IEEE Transactions on Sustainable Energy*, vol. 6, no. 1, pp. 60-69, Jan. 2015.

[12] D. Lusignani, D. Barater, G. Franceschini, G. Buticchi, M. Galea and C. Gerada, "A high-speed electric drive for the more electric engine", 2015 IEEE Energy Conversion Congress and Exposition (ECCE), Montreal, QC, 2015, pp. 4004-4011. doi: 10.1109/ECCE.2015.7310225.

[13] P. Guglielmi, M. Pastorelli, G. Pellegrino and A. Vagati, "Position-sensorless control of permanent-magnet-assisted synchronous reluctance motor", in IEEE Transactions on Industry Applications, vol. 40, no. 2, pp. 615-622, March-April 2004. doi: 10.1109/TIA.2004.824438